Temporal and spatial evolution of picosecond phonon-polariton pulses in crystals

F. Vallée and C. Flytzanis
Laboratoire d'Optique Quantique du Centre National de la Recherche Scientifique, Ecole Polytechnique, 91128 Palaiseau CEDEX, France
(Received 22 June 1992)

The creation and the detection of short polariton pulses by use of the nonlocal time-resolved coherent anti-Stokes Raman scattering (CARS) technique is analyzed using a classical model. The spatiotemporal evolution of the CARS signal is calculated and the relations between the measured parameters and the material characteristics governing the polariton dynamics are explicitly derived. The results are applied to the investigation of the ordinary polariton in $LiIO_3$ on both sides of a forbidden band. The dispersions of the polariton group velocity and dephasing time are directly measured in the time domain and the results are compared to static investigations. The frequency and temperature dependences of the measured polariton dephasing rates are interpreted in terms of anharmonic coupling with phonons on the basis of a theoretical model including both electrical and mechanical anharmonicity.

I. INTRODUCTION

Among the collective excitations of a crystal a particular role is played by the hybrid electromagnetic-material excitations: the polaritons. These composite excitations which in their simplest form arise from the coherent linear interaction of a polar material mode (exciton, phonon, magnon, . . .) with the electromagnetic field, monitor the electromagnetic signal propagation in a material close to its dipole allowed transitions.[1] Information about the underlying dynamics of these quasiparticles and in particular on the processes that condition their relaxation and coherence is thus of both fundamental and technological relevance. Furthermore the concept of polariton relaxation and dephasing is in itself of particular interest because of the composite nature of the excitation. In fact polariton interaction with its environment cannot be *a priori* located on its electromagnetic or material part but, in the most general situation, occurs through both of them.[2]

As a consequence of their partly photon nature, phonon polaritons are characterized by a strong dispersion and consequently a large group velocity. In noncentrosymmetric crystals polariton dispersion has been extensively studied using near forward spontaneous Raman scattering, allowing a precise mapping of polariton static properties under various conditions.[3] Polariton dynamics is, however, much more difficult to access by such a spectral technique and only a few experiments have addressed this problem.[4] The intrinsic difficulty lies in the fast change of polariton frequency with its wave vector partly masking the polariton linewidth and necessitating the use of deconvolution techniques.

In the time domain, relaxation and dephasing of nonpropagating modes of crystals were extensively studied using local coherent techniques based on a local excitation and time-delayed probing of a wave packet. These can be used as long as the wave-packed propagation during its relaxation time can be neglected. This hypothesis holds for most of the pure material excitations but generally fails for polaritons which can propagate over macroscopic distances during the time scale of their decay. Relaxation thus takes place concurrently with escape from the excitation zone requiring the use of adapted techniques. New investigation methods were recently devised allowing the study in real time and space of fast propagating excitations, both in the visible and far-infrared domain and for surface and bulk modes.[5–9]

In the far-infrared domain two main techniques based on second-order processes allow us to address the phonon-polariton pulse dynamics in noncentrosymmetric crystals. These are the electro-optics Cherenkov effect[5] and the nonlocal picosecond time-resolved CARS (coherent anti-Stokes Raman scattering).[6] The former exploits the large frequency width of a femtosecond pulse to excite a low-frequency polariton wave packet through optical rectification. Its spatial and temporal behavior is subsequent followed using a second spatially displaced femtosecond pulse probing the concomitant induced birefringence. The short duration of the pulses compared to the polariton period allows the resolution of the individual polariton oscillations but results in a large frequency content of the wave packet. A careful analysis of the data is thus necessary to extract information on the polariton dynamics and its frequency dependence.[5] More importantly, the method is limited to low-frequency polariton with an upper limit given by the pulse bandwidth (typically 200 cm^{-1}). The picosecond technique we used in this investigation gives only access to the wave-packet envelope but has the advantage of being frequency selective and is particularly suited to high-frequency polaritons (typically ≥ 100 cm^{-1}). This technique is in essence a "time-of-flight" experiment and consists in separating in space the coherent excitation and probing stages of the time-resolved CARS.[6] As outlined in Fig. 1, the coherent excitation of a polariton wave packet is realized at time $t=0$ and position $y=0$ by coherent scattering of two picosecond pulses with frequencies ω_L and ω_S and with wave vectors $\mathbf{k}_L$ and $\mathbf{k}_S$. The frequencies and the experimental geometry are chosen to resonantly excite a polari-

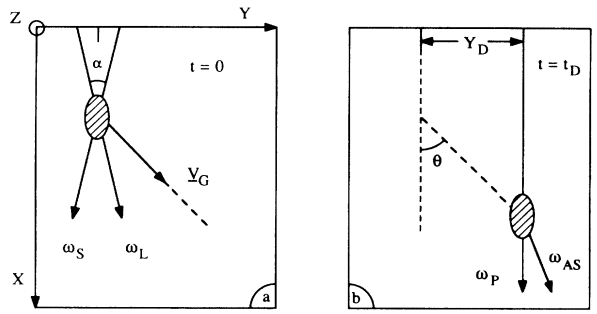

FIG. 1. Principle of the nonlocal time-resolved CARS technique: (a) coherent polariton excitation, (b) coherent polariton detection. The angle α between the excitation beams has been exaggerated for clarity.

ton wave packet with central frequency ω_π and wave vector $\mathbf{k}_\pi$:

$$\omega_L-\omega_s=\omega_\pi,\quad \mathbf{k}_L(\omega_L)-\mathbf{k}_S(\omega_S)=\mathbf{k}_\pi(\omega_\pi)\ . \tag{1.1}$$

Although a linear excitation could also be used, the nonlinear method allows a polariton creation in the bulk of the crystal together with a better control of the initial wave packet through frequency and wave-vector selection (1.1). When the excitation process has terminated, the wave packet freely propagates inside the crystal along a direction fixed by its wave vector $\mathbf{k}_\pi$ and with its group velocity $V_g(\mathbf{k}_\pi)$. Its temporal and spatial evolution is monitored directly in the bulk of the crystal by phase-matched coherent anti-Stokes Raman scattering at $\omega_A=\omega_P+\omega_\pi$ of a third picosecond pulse of frequency ω_P displaced with respect to the excitation in time by t_D and in space by y_D (Fig. 1). The nonlocal probing allows a separation of the temporal and spatial polariton features and gives a direct and independent access to its dephasing time and group velocity. Measurement of the polariton parameters by this technique is analyzed in Sec. II.

The first demonstration of the nonlocal CARS was performed in the ammonium chloride crystal.[6] In such a cubic system, the wave-vector selection associated with Raman techniques limits the measurements to the lower polariton branch.[3] The optical birefringence of anisotropic media permits us to circumvent this limitation, allowing the entire polariton dispersion curve to be accessed.[10] We have used the nonlocal time-resolved CARS technique to investigate the upper and lower ordinary polariton in the vicinity of the highest-frequency reststrahlen band of the uniaxial lithium iodate ($LiIO_3$) crystal. The results are presented in Sec. III and are compared to the analysis of Sec. II. Interpretation of the frequency and temperature dependences of the measured dephasing time is given in Sec. IV together with a model for the anharmonic decay of phonon polaritons.

II. NONLOCAL TIME-RESOLVED CARS

The nonlinear creation and detection of a polariton wave packet by nonresonant electromagnetic fields is analyzed on the basis of the classical Lorentzian model of the polariton. This description is particularly simple in isotropic crystals and in order to avoid any unnecessary complications we limit our analysis to this case. Nevertheless the results are directly applicable to the experimental investigation considered in Sec. III of an ordinary polariton propagating in the ordinary plane of a uniaxial crystal. Here the evolution of the polariton pulse is not influenced by the crystal anisotropy which only plays a role in the propagation of the excitation and probing pulses. Generalization to any more complicated geometry can be easily performed.

Following the Lorentzian model, the polar material excitation is represented by an assembly of noninteracting isotropic harmonic oscillators with frequency ω_0 and displacement amplitude Q_π. As they oscillate they radiate an electric field $\mathbf{E}_\pi$ which interacts with the oscillators. The actual transverse excitation is thus a mixed photon-phonon mode obeying the following set of equations:

$$\frac{\partial^2\mathbf{Q}_\pi}{\partial t^2}+\Gamma\frac{\partial Q_\pi}{\partial t}+\omega_0^2\mathbf{Q}_\pi=\frac{e^*}{\mu}\mathbf{E}_\pi\ , \tag{2.1a}$$

$$\nabla^2\mathbf{E}_\pi-\frac{\epsilon_b}{c^2}\frac{\partial^2\mathbf{E}_\pi}{\partial t^2}=4\pi\frac{e^*N}{c^2}\frac{\partial^2\mathbf{Q}_\pi}{\partial t^2}\ . \tag{2.1b}$$

e^* and μ are the effective charge and mass of the oscillators and N their number density. Γ is a frequency-dependent mechanical coefficient modeling the polariton damping. A unique polar mode is explicitly considered assuming that all other resonances are at much higher or lower frequencies so that their contribution can be lumped in a real frequency-independent dielectric constant ϵ_b. By Fourier transforming equations (2.1) the polariton dispersion in a cubic crystal is obtained:[1]

$$\frac{k_\pi^2c^2}{\omega_\pi^2}=\epsilon(\omega_\pi)=\epsilon_b\left[1+\frac{\Omega_p^2}{\omega_0^2-\omega_\pi^2-i\Gamma\omega_\pi}\right]\ , \tag{2.2}$$

where Ω_p is the plasma frequency:

$$\Omega_p^2=4\pi Ne^{*2}/\mu\epsilon_b\ . \tag{2.3}$$

Apart from the transverse excitation a longitudinal mode is also formed with frequency ω_{LO}:

$$\omega_{LO}^2=\omega_{TO}^2+\Omega_p^2\ . \tag{2.4}$$

No mode can propagate in the $\omega_{LO}-\omega_{TO}$ frequency region (reststrahlen or forbidden band). In the following we will assume a weak polariton damping ($\Gamma\ll\omega_0-\omega_\pi$) which corresponds to the experimental conditions of Sec. III. The real and imaginary parts k'_π and k''_π of the ω_π polariton wave vector can thus be written

$$k'_\pi=\frac{\omega_\pi}{c}\left[\epsilon_b\left[1+\frac{\Omega_p^2}{\omega_0^2-\omega_\pi^2}\right]\right]^{1/2}\ , \tag{2.5a}$$

$$k''_\pi=\frac{\epsilon_b\omega_\pi^3\Omega_p^2\Gamma}{2k'_\pi c^2(\omega_0^2-\omega_\pi^2)^2}\ . \tag{2.5b}$$

These parameters govern the polariton dispersion and absorption and are accessed in spectral experiments. In the time domain their counterparts are polariton propagation and relaxation measured by the polariton group velocity

V_g and by the polariton dephasing time T_2:

$$V_g=\frac{\partial\omega_\pi}{\partial k'_\pi}\ , \tag{2.6a}$$

$$T_2=(V_g k''_\pi)^{-1}\ , \tag{2.6b}$$

which are the parameters of interest here.

As indicated above the creation of a short polariton wave packet is realized by coherent scattering of two synchronized picosecond pulses, E_L and E_S, whose frequencies, ω_L and ω_S, lie in the transparency region of the sample. Polariton interaction with the incident fields occurs through both of its components and can be described by a phenomenological energy density:[11]

$$U=-\mathbf{d}_E\mathbf{E}_L\mathbf{E}_S^*\mathbf{E}_\pi^*-N\mathbf{d}_Q\mathbf{E}_L\mathbf{E}_S^*Q_\pi^*+\text{cc}\ , \tag{2.7}$$

where $\mathbf{d}_E$ and $\mathbf{d}_Q$ are third-order coupling tensors which vary only slowly with frequency. They account for, respectively, the nonresonant optical coupling and the resonant interaction with the material excitation. The actual polariton-optical pulse interaction is thus a coherent superposition of parametric amplification and coherent Raman scattering.[12] Selection rules are identical for these two mechanisms and can be deduced from the symmetry of the second-order susceptibility in the investigated material. In particular, both of the coupling parameters vanish in centrosymmetric media, limiting the applicability of the technique to noncentrosymmetric materials.

In such a medium the nonlinear polarization P_{NL} and force F_{NL} acting, respectively, on the electrical and mechanical parts of the polariton are obtained by suitable derivation of the energy density. For undepleted incident pulses the polariton excitation is governed by the following set of equations:

$$\frac{\partial^2 Q_\pi}{\partial t^2}+\Gamma\frac{\partial Q_\pi}{\partial t}+\omega_0^2 Q_\pi=\frac{e^*}{\mu}\mathbf{E}_\pi+\frac{1}{\mu}\mathbf{F}_{\text{NL}}\ , \tag{2.8a}$$

$$\nabla^2\mathbf{E}_\pi-\frac{\epsilon_b}{c^2}\frac{\partial^2\mathbf{E}_\pi}{\partial t^2}=4\pi\frac{e^*N}{c^2}\frac{\partial^2 Q_\pi}{\partial t^2}+\frac{4\pi}{c^2}\frac{\partial^2\mathbf{P}_{\text{NL}}}{\partial t^2}\ . \tag{2.8b}$$

In order to fix the experimental geometry, we assume that a polariton wave packet with central frequency ω_π and wave vector k_π is resonantly excited [i.e., conditions (1.1) are satisfied]. Provided that the refractive indexes at ω_L and ω_s are known, wave-vector conservation imposes the angle α between the incident pulses and consequently the propagation direction of the polariton [typically $\theta\sim 45°$ (Fig. 1)]. The incident plane is identified with the (x,y) plane and the spatial origin is fixed at the crossing point of the excitation beams. Noting that α is small ($\sim 2°$) and that the confocal parameters of the focusing lenses are large compared to the interaction length, the incident fields may be written in the form

$$\mathbf{E}_{L,S}(\mathbf{r},t)=\hat{e}_{L,S}\,A_{L,S}(\mathbf{r}_\perp^{L,S},t-x/u)\exp i(\mathbf{k}_{L,S}\cdot\mathbf{r}-\omega_{L,S}t)\ , \tag{2.9}$$

where $\hat{e}_{L,S}$ is the direction of polarization of the $E_{L,S}$ fields. The dispersion of the light group velocity u has been neglected and the amplitude variation over the transverse coordinate ($\mathbf{r}_\perp^{L,S}$) accounts for the spatial shape of the incident beams. A Gaussian transverse profile is assumed for the field amplitudes $A_{L,S}$, in agreement with the experimental geometry of Sec. III. The variation of the beam overlap over the interaction region can thus be lumped in a crossing function $H(x)$:

$$H(x)=\exp\left[-\frac{2x^2\sin(\alpha/2)}{a_0^2}\right]\ , \tag{2.10}$$

where a_0 is the beam waist radius. For a polariton along $\hat{e}_\pi$, P_{NL} and F_{NL} are thus proportional to

$$E_{\text{NL}}(\mathbf{r},t)=A_L(y,z,t-x/u)A_S^*(y,z,t-x/u)H(x)\times\exp i[(\mathbf{k}_L-\mathbf{k}_S)\cdot\mathbf{r}-(\omega_L-\omega_s)t]\ . \tag{2.11}$$

The mechanical and electrical parts of the polariton can be calculated using their Fourier components:

$$\mathbf{E}_\pi(\mathbf{r},t)=\hat{e}_\pi\int_{-\infty}^{+\infty}A_\pi(\mathbf{r},\nu)\exp i[\mathbf{k}'_\pi(\omega_\nu)\cdot\mathbf{r}-\omega_\nu t]d\nu \tag{2.12}$$

with $\omega_\nu=\omega_\pi+\nu$. A similar expression is used for $\mathbf{Q}_\pi$. Using Eqs. (2.8), (2.11), and (2.12) and assuming a weak focalization of the incident beams in a crystal long compared to the interaction length, the Fourier components of the electric part of the polariton are given by

$$A_\pi(x,y,z,\omega_\nu)=\beta_\nu\exp(-k''_\nu z/\cos\theta)\times\int_{-\infty}^{z}\exp(k''_\nu w/\cos\theta)\times A_{\text{NL}}[y-(x-w)tg\theta,\omega_\nu]H(w)\times\exp(i\Delta k_\nu w)dw\ , \tag{2.13}$$

where the following abbreviations were used:

$$\beta_\nu=\frac{2i\pi}{c^2 k'_\nu}\omega_\nu^2\ , \tag{2.14a}$$

$$k''_\nu=k''_\pi(\omega_\nu),\quad k'_\nu=k'_\pi(\omega_\nu)\ , \tag{2.14b}$$

$$\Delta k_\nu=\nu u^{-1}-(k'_\nu-k'_0)\sim[u^{-1}-V_g^{-1}\cos^{-1}\theta]\nu\ , \tag{2.14c}$$

$$d(\omega_\nu)=\mathbf{d}_E\hat{e}_L\hat{e}_S\hat{e}_\pi+\frac{Ne^*\mathbf{d}_Q\hat{e}_L\hat{e}_S\hat{e}_\pi}{\mu(\omega_0^2-\omega_\nu^2-i\omega_\nu\Gamma)}\ , \tag{2.14d}$$

$$A_{\text{NL}}(y,\omega_\nu)=d(\omega_\nu)\int_{-\infty}^{+\infty}A_L(y,z,\nu')A_L^*(y,z,\nu'-\nu)d\nu'\ . \tag{2.14e}$$

Here $A_L(\omega)$ and $A_S(\omega)$ are the Fourier components of the excitation field amplitudes. The wave packet is fully determined by expressions (2.12) and (2.13) together with (2.14). The result can be simplified by introduction of the polariton group velocity V_g provided that the group velocity dispersion over the spectral width $\delta\nu$ of the polariton wave packet is small, i.e.,

$$\delta\nu\ll|\omega_0-\omega_\pi|\ . \tag{2.15}$$

$\delta\nu$ is limited both by wave-vector selection and by the frequency content of the excitation (2.13). The former selection process is particularly efficient for a small polariton group velocity (2.14c), i.e., in the vicinity of ω_0, strongly

limiting the polariton extension in the ω space. As the group velocity increases the k selection weakens and may become ineffective if group velocity matching is realized ($u = V_g \cos\theta$), i.e., if the dispersion of $|k_L - k_S|$ exactly matches the polariton dispersion.[13] k-selection weakening is compensated by frequency selection whose efficiency (in the k space) increases with increasing group velocity. In fact the combination of k- and ω-space selection allows condition (2.15) to be always met in our experiment.

The above analysis holds only if the dispersion of the coupling term $d(\omega_\nu)$ can be disregarded over $\delta\nu$. This approximation may generally be performed except in the region of strong destructive interferences between the electrical and mechanical coupling of the polariton with the incident fields which occur either below or above ω_{TO}, depending on the relative sign of $\mathbf{d}_E \hat{e}_L \hat{e}_S \hat{e}_\pi$ and $\mathbf{d}_Q \hat{e}_L \hat{e}_S \hat{e}_\pi$ (2.14d). Close to the minimum of $d(\omega_\nu)$, a strong spectral broadening of the excited polariton wave packet occurs due to the compensation of the k and ω selection by the simultaneous $d(\omega_\nu)$ variation, rendering the applicability of the group velocity concept questionable. Such a broadening was first pointed out by Benson and Mills in near forward spontaneous Raman scattering.[13] As this occurs close to a very particular polariton frequency this case will not be considered in the following.

Introducing the group velocity and neglecting the dispersion of β_ν and k''_ν on the wave-packet width one obtains

$$A_\pi(x,y,t') = \beta \exp(-t'/T_a) \int_{-\infty}^{t'} \exp(\tau/T_a) A_{NL}[y + (\tau - t')V_a \sin\theta, \tau] H[x + (\tau - t')V_a \cos\theta] e^{i\Delta\mathbf{k}\cdot\mathbf{r}} d\tau \ . \tag{2.16}$$

t' is the retarded time ($t' = t - x/u$) and $A_{NL}(y,\tau)$ is a temporal excitation function defined as

$$A_{NL}(Y,\tau) = \int_{-\infty}^{+\infty} A_{NL}(Y,\omega_\nu) e^{-i\nu\tau} d\nu \ . \tag{2.17}$$

The apparent polariton dephasing time T_a and apparent velocity V_a are related to the real dephasing time and group velocity by

$$T_a = (1 - V_g u^{-1} \cos\theta)/V_g k''_0 \ , \tag{2.18a}$$

$$V_a = V_g/(1 - V_g u^{-1} \cos\theta) \ . \tag{2.18b}$$

Expression (2.16) for the electrical amplitude of the polariton shows that the excitation buildup results from accumulation of the elementary excitations created at different time and place inside the crystal reaching the point $\mathbf{r}$ at time t after propagation with the group velocity V_g. This spatiotemporal accumulation over the temporal duration of the excitation process results in both a spatial and temporal displacement of the maximum amplitude of the wave packet as compared to the spatial and temporal overlap of the incident pulses.

For long time t' (i.e., $t' \gg t_p$ where t_p is the duration of the pulses) the electric field amplitude can be written in a closed form:

$$A_\pi(\mathbf{r},t) = e^{-t'/T_a} B(\mathbf{r} - \mathbf{V}_a t') \ . \tag{2.19}$$

This expression indicates a free propagation of the polariton wave packet in a direction determined by the angle θ and with the apparent velocity $V_a(\omega_\pi)$. As the polariton propagates its amplitude is exponentially damped with a characteristic time T_a.

The temporal and spatial features of the polariton can be directly accessed in the real space by coherent anti-Stokes Raman scattering of a third picosecond probe pulse E_P with frequency ω_P (Fig. 1). The incident direction of the probe is imposed by overall phase matching condition: $\mathbf{k}_{AS} = \mathbf{k}_L - \mathbf{k}_S + \mathbf{k}_P$ fixing the experimental geometry. As the phase matching angle for the probe beam is small ($\sim 1°$) the probe field can be written in the same form as the excitation ones (2.9). The generation of the anti-Stokes signal is described by the usual nonlinear propagation equation:

$$\nabla^2 \mathbf{E}_{AS} - \frac{n_{AS}^2}{c^2} \frac{\partial^2 \mathbf{E}_{AS}}{\partial t^2} = \frac{4\pi}{c^2} \frac{\partial^2 \mathbf{P}_{NL}}{\partial t^2} \ , \tag{2.20}$$

where the source term P_{NL} is calculated from an energy density similar to (2.8):

$$\mathbf{P}_{NL} = -\mathbf{d}_E \mathbf{E}_P \mathbf{E}_\pi - N \mathbf{d}_Q \mathbf{E}_P \mathbf{Q}_\pi + \text{cc} \ . \tag{2.21}$$

The spatial and temporal behavior of the intensity of the coherent signal is readily calculated using (2.13):

$$S_{AS}(y_D,t_D) = |\beta\gamma|^2 \frac{cn_{AS}}{8\pi} L_{\text{eff}}^2 \exp(-2t_D/T_a)$$

$$\times \int_{-\infty}^{+\infty} dt \int_{-\infty}^{+\infty} dy \int_{-\infty}^{+\infty} dz \, |A_P(y,z,t)|^2 \exp(-2t/T_a)$$

$$\times \left| \int_{-\infty}^{t+t_D} d\tau \exp(\tau/T_a) A_{NL}[V_a(\tau - t - t_D) + y + y_D, z, \tau] \right|^2 \ , \tag{2.22}$$

where

$$\gamma=\frac{2i\pi\omega_{AS}^2}{k_{AS}c^2}\left[\mathbf{d}_E\hat{e}_{AS}\hat{e}_P\hat{e}_\pi+\frac{Ne^*\mathbf{d}_Q\hat{e}_{AS}\hat{e}_P\hat{e}_\pi}{\mu(\omega_0^2-\omega_\pi^2)}\right] \quad (2.23)$$

and L_{eff} is the effective interaction length.

The spatial and temporal dependences of the signal intensity directly reflect the wave-packet evolution. For long time delay ($t_D \gg t_P$) the excitation process has terminated and hence the last integral in (2.22) is constant. The signal intensity can thus be written as the product of a damping function with the propagation function of the envelope of the polariton pulse:

$$S_{AS}(y_D,t_D)=\exp(-2t_D/T_a)C(y_D-V_a t_D) . \quad (2.24)$$

The polariton propagation and relaxation features are thus separated and probed by independent parameters. For a fixed probe delay the determination of the spatial maximum $y_M(t_D)$ of the signal gives access to the apparent velocity $V_a=y_M(t_D)/t_D$. Using the value of θ determined from wave-vector conservation (1.1) and $u=c/n$ one thus directly measures the polariton group velocity:

$$V_g=(V_a^{-1}\sin\theta+nc^{-1}\cos\theta)^{-1} . \quad (2.25)$$

The polariton damping can be measured by simultaneously altering the probing time and probing point in order to follow the polariton propagation in the transverse direction. With the polariton model used above an exponential decay of the signal is expected with the apparent dephasing time T_a from which the real polariton dephasing time T_2 can be obtained:

$$T_2=T_a/(1-V_g u^{-1}\cos\theta) . \quad (2.26)$$

The apparent polariton parameters are measured in our experiment because of the polariton propagation along the longitudinal direction. The probe pulse needs a significant time to catch up the polariton modifying the actual probe time delay and thus the measured time-dependent features. For long delay the previous relation connecting the measured and real polariton parameters can be established using simple geometrical considerations.[6]

In order to obtain a more detailed description of the polariton evolution we have performed a numerical evaluation of the coherent signal for an arbitrary time delay. The temporal and spatial shape of the incoming pulses are taken as Gaussian with widths relevant to our experimental system (see Sec. III). Typical material parameters were used: $V_g=c/8$, $q=45°$, $u=\frac{2}{3}c$ and $T_a=20$ ps. The spatial dependence of the signal calculated for three different probe delays is shown in Fig. 2. For small delay the signal quickly grows up and broadens to reach its maximum around $t_D=\frac{2}{3}t_p$ (~ 2 ps). This broadening is a consequence of polariton propagation during the finite duration of the excitation process, leading to a polariton spatial shape slightly larger than the superposition of the focal spots. For larger delay the signal amplitude decreases but its spatial shape remains unchanged. As pointed out earlier, the maximum of the signal is displaced with respect to the spatial origin $y_D=0$, emphasizing the accumulation nature of the excitation process. This is similar to the temporal accumulation observed in the usual local CARS technique.[14]

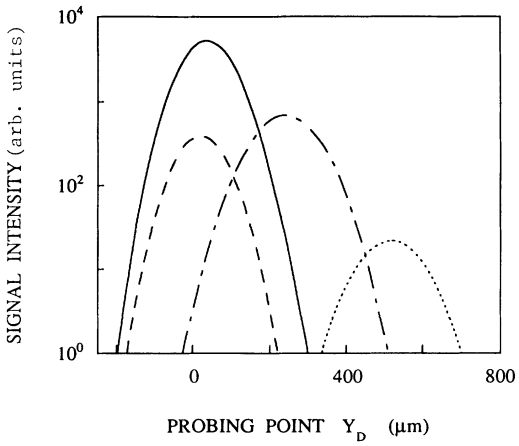

FIG. 2. Calculated CARS signal on a logarithmic scale as a function of probing position (Y_D) for four different probe delays: −3 (dashed line), 0 (full line), 9 (dash-dotted line), and 18 ps (dotted line).

The temporal dependence of the spatial position $y_M(t_D)$ of the signal maximum is plotted in Fig. 3 for three different values of T_2. As expected a linear variation is predicted for long time delay corresponding to a free propagation of the polariton with its apparent velocity. A strong deviation from the linear dependence is observed for delay shorter than the pulse duration. This results from the competition between the polariton escape from the excitation zone and its local excitation at the crossing point of the incident pulses. As T_2 decreases the influence of the polaritons produced by the leading edge of the excitation pulses decreases and the initial regime dominated by polariton generation is observed for a longer time. We emphasize that this apparent polariton slowing down is masked whenever the instantaneous non-

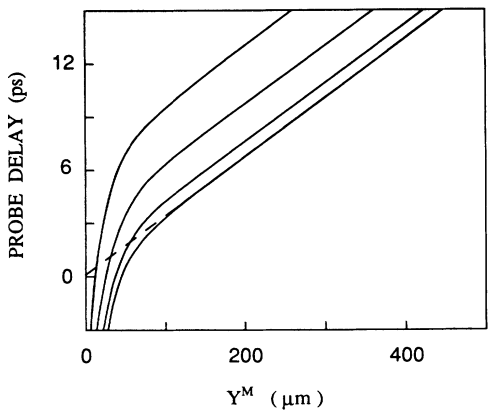

FIG. 3. Calculated dependence between the position (Y^M) of the maximum of the signal and the probe delay for four different values of the polariton dephasing rate: $T_2/2=12$, 3, 1, and 0.5 ps (from bottom to top).

resonant nonlinear contribution of the crystal dominates the small delay signal. In this case the maximum of the signal coincides with the spatial and temporal origin so that for sufficiently long dephasing times the measurements can be described by a straight line passing through the origin.[6] The temporal evolution of the peak coherent signal is very similar to the one observed in local time-resolved CARS (Ref. 14) except that the exponential decay for long time delays of the probe measures the apparent dephasing time T_a.

It is interesting to compare the results of the time- and space-resolved CARS to those obtained by use of local techniques such as near forward spontaneous Raman scattering. In this technique the polariton characteristics are accessed in the (k,ω) space by measuring the Stokes shift of an incident pulse of frequency ω_L as a function of the scattering direction. The polariton relaxation can be addressed by performing linewidth measurement for a fixed scattering direction. With the hypothesis of a small damping the spectral profile of the Stokes line is given by[3]

$$A_\alpha(\omega_S)\sim\frac{\gamma/2}{[\omega_S-\omega_S(\alpha)]^2+(\gamma/2)^2}\ . \tag{2.27}$$

$\omega_S(\alpha)$ is the Stokes frequency in the α direction as given by the conservation rules (1.1). For an angle α defined with an infinite precision one obtains a Lorentzian line with a full width at half maximum (FWHM) γ.

$$\gamma=\frac{\omega_\pi\epsilon''}{c\epsilon'^{1/2}|nc^{-1}\cos\theta-V_g^{-1}|}\ . \tag{2.28}$$

The group velocity dependence of γ reflects the change in the scattering conditions with the polariton frequency (i.e., the relative slope of the dispersion of k_π and $|\mathbf{k}_L-\mathbf{k}_S|$) and is the counterpart of the longitudinal polariton propagation in the time domain. γ is thus directly connected to the apparent dephasing time: $\gamma=2/T_a$. As expected, the spectral and temporal Raman techniques measure related parameters and in particular the modification of the apparent dephasing time due to polariton propagation in the time and space domain has a direct correspondence in the wave-vector and frequency domain as it is associated to an intrinsic polariton broadening induced by its dispersion.

Spontaneous Raman scattering was only scarcely applied to the measurements of polariton linewidth because of the intrinsic difficulty of the experiments.[4] Any finite width of the investigated polariton in the k space adds an instrumental width to the measured signal necessitating a deconvolution procedure to extract the real linewidth since the dispersion and the frequency broadening of the polariton are measured by the same experimental observable. Measurements are easier for a large polariton broadening, rendering spontaneous Raman and nonlocal time-resolved CARS very complementary techniques, the latter being particularly suited to long living polaritons ($T_2>1$ ps).

III. RESULTS IN $LiIO_3$

In cubic crystals the energy and wave-vector conservations (2.1) limit the Raman techniques to the lower polariton branch ($\omega_\pi<\omega_{TO}$) with a minimum polariton wave vector:[3].

$$k_\pi=(n_L\omega_L-n_s\omega_S)\sim\frac{(\epsilon_b)^{1/2}}{c}\omega_\pi\ . \tag{3.1}$$

In anisotropic media this limitation can be overcome by use of the birefringence. Using suitable orientation of the crystal and polarizations of the laser and Stokes beams no minimum value of k_π is imposed, allowing the investigation of both the upper and lower branch polariton.[10] We have taken advantage of this to investigate the ordinary polariton in lithium iodate in the vicinity of its highest-frequency polar mode by use of the nonlocal CARS technique.

The α phase of $LiIO_3$ belongs to the C_6^6 group with two molecules per unit cell allowing A, E_1, E_2, and B symmetry modes. A and E_1 modes are both infrared and Raman active, E_2 modes are only Raman active,[15–17] while B modes are both infrared and Raman silent but can be observed in hyper-Raman scattering.[18] All these modes were extensively investigated and their frequencies are known with a good accuracy. The A and E_1 polar modes permit the observation of phonon polaritons whose dispersion curves were investigated by near forward Raman scattering and are very well described by theoretical formula.[10] Ordinary polaritons are associated with the E_1 phonons (polarization in the x-y plane) with a highest-frequency mode identified as an internal vibration of the iodate ions ($E_{1TO}=768$ cm^{-1}, $E_{1LO}=843$ cm^{-1}).[16]

The three independent picosecond pulses for the CARS-type experiment are created from a single 5-ps pulse delivered by a passively mode-locked cavity dumped Nd/glass oscillator. After amplification to 2 GW the infrared pulse at 1.054 μm is doubled in frequency in a potassium dihydrogen phosphate (KDP) crystal. The green and infrared beams are separated using a dichroic mirror, the remaining infrared being doubled in a second KDP crystal to pump a dye amplifier. The visible pulse is divided into three parts. The first two are frequency shifted by stimulated Raman scattering in, respectively, deuterated methanol and ethanol to create the ω_L and ω_P beams. The last part is tightly focused into a methanol cell to generate a picosecond quasicontinuum from which a narrow frequency band is selected by a grating and amplified in a dye amplifier. This creates the second excitation beam ω_S which is tunable. The three pulses are shifted from the initial frequency to facilitate phase matching and to enable polariton excitation over a larger part of its dispersion curve with the same crystal orientation. The three pulses have Gaussian temporal shapes with a width of 3 ps for ω_L and ω_P and 5 ps for ω_S. The use of different frequencies for the three input pulses allows a very good signal over noise ratio and a very high sensitivity. The temporal resolution of the system is routinely of 0.4 ps and the spectral bandwidth of the pulses is of the order of 10 cm^{-1}. After polarization adjustment the beams are focused with 20-cm lenses into the $LiIO_3$ sample with a calculated noncollinear geometry. The anti-Stokes signal is detected by a photomultiplier after spectral and polarization selections al-

lowing a very high signal over noise discrimination.

The $LiIO_3$ sample is an x-ray oriented 7-mm-thick crystal. It was placed in a liquid-nitrogen- or helium-cooled cryostat with its optic axis perpendicular to the plane of incidence of the pulses. The geometry of the experiment was chosen to impose polariton wave vector and polarization in the (x,y) plane which obviates any influence of the extraordinary polariton. Most of the measurements were performed with an ordinary polarized ω_L beam and with an extraordinary polarized ω_S beam permitting a large portion of the polariton dispersion curve to be accessed. In such a negative uniaxial crystal this corresponds to $k_S > k_L$ and hence the polariton is counterpropagating inside the crystal (1.1). To investigate large wave-vector polaritons around ω_{TO} all the polarizations were rotated by 90° allowing the creation and detection of the 760-cm^{-1} polariton with small angles between the input beams.

The measured spatial and temporal dependence of the 680 cm^{-1} polariton wave packet is shown in Fig. 4 where the intensity of the anti-Stokes signal has been plotted on a logarithmic scale as a function of probing position y_D for the three probe time delays $\Delta t_D \equiv 0$, 6.5, and 13 ps (where the delay is measured from the temporal maximum of the signal). The position of the spatial maximum clearly shifts with t_D demonstrating the polariton propagation. The transverse shape of the excitation images the initial almost Gaussian shape and can be reproduced by the theoretical curves calculated from (2.22) (full lines). This good agreement suggests that spatial broadening of the initial wave packet during its propagation is small. The spatial response of the system has been measured in a glass ensuring near phase matching with the same geometry. As expected, the nonresonant signal is spatially peaked at the excitation point whatever the probe delay and its intensity decreases faster following the system response function.

The observation of the signal over several orders of magnitude allows a very good spatial resolution of the order of 20 μm for a focal spot diameter of 100 μm (FWHM). Therefore we can precisely determine the central position of the wave packet for various probe delay and the results are shown in Fig. 5. As expected, a linear dependence is observed for long time delay ($t_D > 3$ ps) the slope of which gives access to the apparent polariton velocity and thus to its group velocity: $V_g(680\ cm^{-1}) = (0.13 \pm 0.15)c$, using $\theta(680\ cm^{-1}) = 135°$.

In lithium iodate the nonresonant third-order susceptibility gives a negligible contribution to the small delay signal so that the initial resonant regime can be observed ($t_D < 3$ ps). The results were fitted using expression (2.22) where the spatial and temporal origins are chosen such that the theoretical and experimental maximum of the signal coincides (second point in Fig. 5). The experimental data are correctly reproduced using the previous value of the group velocity and a dephasing time of 3.3 ps at 80 K. In fact the dephasing time only influences the small delay part of the curve and is independently determined (see below).

Measurements were performed for various polariton frequencies on both sides of the reststrahlen band. For polariton above the longitudinal mode we have observed an important decrease of the coherent signal with polariton frequency. This was already observed in Raman experiments[19] and results from the decrease of the coupling coefficient due to destructive interferences between the mechanical and electrical coupling of the polariton with the excitation pulses [$|\beta\gamma|$ term in (2.22)]. As this effect has been investigated in earlier experiments and does not play an important role in the polariton dynamics for polaritons far from the coupling minimum, it will not be de-

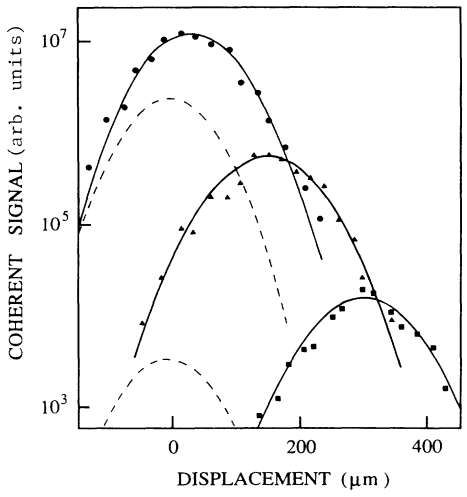

FIG. 4. Spatial dependence of the CARS signal from the 680-cm^{-1} polariton in $LiIO_3$. The probe delay Δt_D measured from the temporal maximum of the signal is 0 (points), 6.5 (triangles), and 13 ps (squares). The full lines are calculated (see text). The dashed lines show the system response function measured in glass for a probe delay of 0 and 5 ps (from top to bottom).

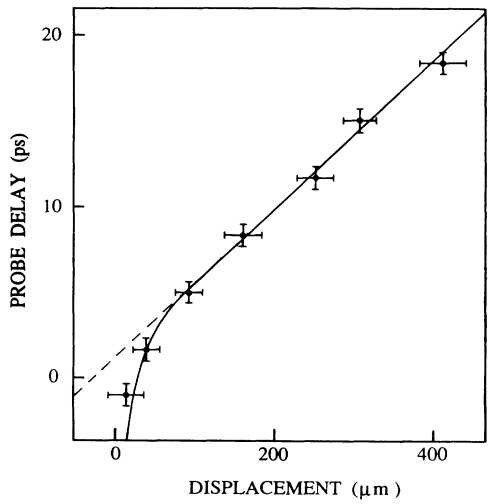

FIG. 5. Measured position of the signal maximum as a function of probe delay for the 680-cm^{-1} polariton in $LiIO_3$. The full line is calculated and allows the determination of the polariton group velocity: $V_g(680\ cm^{-1}) = (0.13 \pm 0.15)c$.

scribed in detail here. The results of the group velocity measurements are shown in Fig. 6. Polariton slowing down in the vicinity of the transverse and longitudinal frequency is clearly observed and reflects the increasing phonon character of the excitation as the reststrahlen branch is approached. The polariton group velocity can be independently estimated by differentiating the dispersion curve measured in spontaneous Raman scattering. This leads to the full line of Fig. 6 which closely describes the experimental points over the whole frequency range studied. Note that the agreement between the static and dynamic measurements is obtained without any parameter.

The temporal evolution of the amplitude of the wave packet is monitored by the temporal dependence of the intensity of the coherent signal, giving access to the polariton relaxation. The variation of the signal maximum with probe delay is depicted in Fig. 7 for the 720-cm^{-1} polariton. Here the probe delay and probing point are simultaneously changed in order to follow the polariton as it propagates in the crystal. After a rapid rise, an exponential decay of the peak signal is observed over five orders of magnitude indicating a homogeneous broadening of the polariton. The real dephasing time can thus be measured from the long time decay: $T_2(720\ cm^{-1})=3.8\pm0.4$ ps at a crystal temperature of 80 K. A detailed description of the data is obtained using (2.22) (full line of Fig. 7).

The polariton relaxation can be measured both as a function of polariton frequency and crystal temperature. The frequency dependence of the dephasing rate $\Gamma_\pi=2/T_2$ is shown in Fig. 8 for a crystal temperature of 80 K. Γ_π decreases in the vicinity of the reststrahlen band with a minimum value around the ω_{TO} frequency. The 760-cm^{-1} polariton dephasing rate measured at 80 K and at room temperature is slightly smaller than the one estimated for the transverse phonon from spontaneous Raman data assuming a Lorentzian line shape ($\omega_{TO}=768\ cm^{-1}$).[17] As the photon part of the 760-cm^{-1} polariton is small ($\sim 1\%$ as measured by the phonon strength factor[1]) this variation cannot be ascribed to a change in the polariton nature and suggests that the minimum of the dephasing rate occurs in the vicinity of 760 cm^{-1}. Also shown in Fig. 8 is the measured dephasing rate of the longitudinal nonpropagating mode at 843 cm^{-1}, in good agreement with spontaneous Raman data.[17] The shape of the frequency dependence of the dephasing rate remains almost unchanged as crystal temperature is increased or lowered but with a large variation of the absolute value of the decay rates. The measured temperature dependence is displayed in Figs. 9 and 10 for two particular polariton frequencies, 680 and 880 cm^{-1}, respectively, below and above the reststrahlen band. For these two polaritons a finite dephasing rate is extrapolated at 0 K and a strong increase of Γ_π is observed with temperature.

The measured wave-packet decay is determined by both the intrinsic properties of the crystal and external

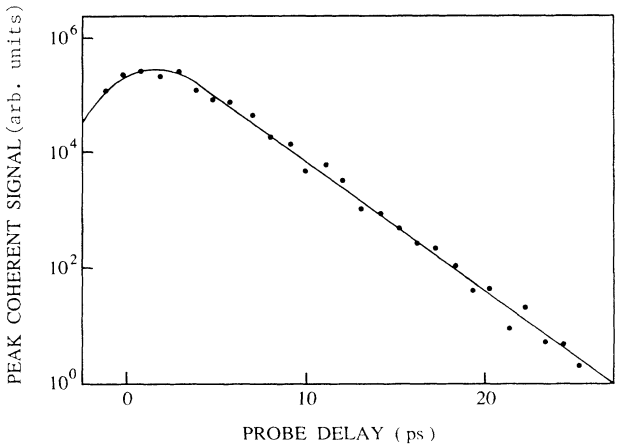

FIG. 7. CARS signal from the "followed" 720-cm^{-1} polariton plotted on a logarithmic scale as a function of probe delay. The temperature of the $LiIO_3$ crystal is 80 K. The exponential decay of the signal measures the polariton dephasing time $T_2/2=1.9\pm0.2$ ps.

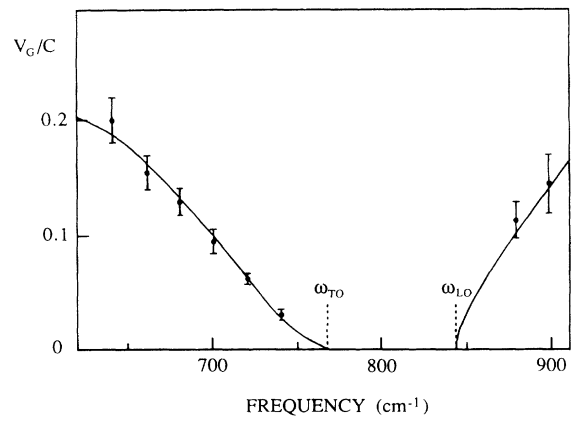

FIG. 6. Dispersion of the polariton group velocity in $LiIO_3$ in the vicinity of the highest-frequency reststrahlen band. The full line is derived from the polariton dispersion curve measured in spontaneous Raman scattering experiments.

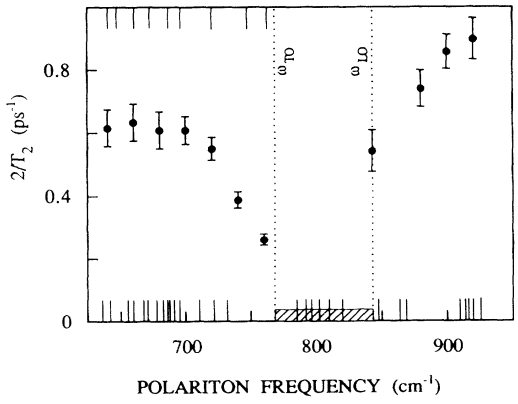

FIG. 8. Measured dispersion of the polariton dephasing rate $\Gamma=2/T_2$ on both sides of the highest-frequency reststrahlen band (shaded region) in $LiIO_3$ at 80 K. Also shown is the measured ω_{LO} dephasing rate. The small lines at the bottom (top) of the figure indicate the allowed down- (up-) conversion processes.

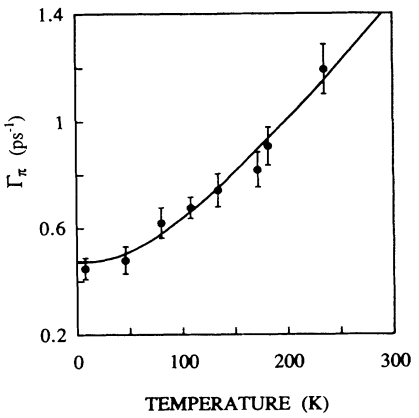

FIG. 9. Temperature dependence of the dephasing rate of the 680-cm^{-1} polariton in $LiIO_3$. The full line is calculated using a down- and up-conversion channel (4.22a).

mechanisms due to the experimental geometry. Under certain experimental conditions external contributions can play a major role in the observed decay. In particular, the polariton wave packet can be temporally and spatially spread by group velocity dispersion and by polariton distribution in the k space. The importance of these effects can be easily estimated using the known experimental geometry and the results show that they give a small contribution (a few percent) for polaritons propagating over short distances (typically less than 1 mm). This is the case in our experiment where the signal decays by a much larger amount (three to four orders of magnitude) over such a distance. A second mechanism is polariton escape from the crystal during its propagation as observed in real space and time in previous experiments.[20] The efficiency of this process strongly depends on the experimental geometry and can be rendered ineffective using a crystal long compared to the length of the excited zone and to the longitudinal propagation distance of the excitation. The intersection of the excitation beams in the crystal results in a short excitation zone with a typical length of 1 mm. We have used a 7-mm-thick crystal and focalized the excitation beams close to the exit surface of the sample (the polariton is counterpropagating) in order to obviate any influence of polariton escape on the measured decay. In our experiment, the measured polariton decay can thus be ascribed to the intrinsic properties of the media and will be interpreted in terms of polariton anharmonic coupling with its environment in Sec. IV.

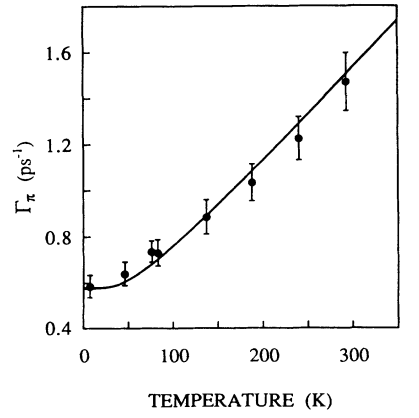

FIG. 10. Temperature dependence of the dephasing rate of the 880-cm^{-1} polariton in $LiIO_3$. The full line is calculated using only a down-conversion channel (4.22b).

IV. POLARITON RELAXATION

In Sec. II polariton relaxation was introduced in a phenomenological way by adding a friction term to the harmonic oscillator describing its mechanical part. This constitutes an important simplification of the problem particularly when damping is investigated over a large frequency range. A more meaningful treatment must start with the polariton as the initial entity and introduces the relaxation as a consequence of its anharmonic interactions with other elementary excitations of the crystal. Scattering by defects or impurities can also play an important role but will not be considered here assuming that the crystal is perfect.[6] The relaxation can thus be analyzed similarly to phonon relaxation in perfect crystals except that the hybrid nature of the initial state introduces some new features. As for phonons,[21] the modifications of the polariton properties by the anharmonic interactions is most precisely described using quantization of the interacting modes and we will use this approach.

As in Sec. II, we assume that in the frequency region of interest the polarizaton effect is dominated by a unique polar mode labeled i_0. In the harmonic approximation the Hamiltonian H_0 describing the linear interaction of the photons with the polar phonon mode can be diagonalized by introduction of the creation and annihilation operators of a polariton with wave vector k and polarization λ, $\alpha^\dagger_{\rho,\lambda}(k)$, and $\alpha_{\rho,\lambda}(k)$, respectively,[22]

$$H_0=\sum_{\rho,k,\lambda}\hbar\omega_{\rho,\lambda}(k)\alpha^\dagger_{\rho,\lambda}(k)\alpha_{\rho,\lambda}(k)\ . \tag{4.1}$$

$\rho=1,2$ labels, respectively, the lower and upper polariton branch and $\hbar\omega_{\rho\lambda}(k)$ is the energy of the ρ polariton with wave vector k and polarization λ. In the following we will only consider a particular polariton polarization and hence the polarization index will be dropped. The polariton operators are simple linear combinations of the bare photon and phonon creation and annihilation operators $(a^\dagger_k,a_k)$ and $(b^\dagger_{i_0k},b_{i_0k})$, respectively,

$$b_{i_0k}=\sum_\rho\left[u_{\rho k}\alpha_{\rho k}+v^*_{\rho-k}\alpha^\dagger_{\rho-k}\right]\ , \tag{4.2a}$$

$$a_k=\sum_\rho\left[u'_{\rho k}\alpha_{\rho k}+v'^*_{\rho-k}\alpha^\dagger_{\rho-k}\right]\ . \tag{4.2b}$$

$u_{\rho k}$, $v_{\rho k}$, $u'_{\rho k}$, and $v'_{\rho k}$ are the coefficients of the linear transformation diagonalizing the initial linear Hamiltonian.[22]

Anharmonic interactions of the polariton with other excitations of the crystal renormalize the polariton energy introducing a polariton damping. Here we will limit our investigation to three-particle interactions which are the lowest-order processes. Two mechanisms are possible

corresponding either to polariton down conversion where the initial polariton dissociates into two lower-energy phonons or to polariton up conversion where the polariton is scattered by a thermal phonon into a higher-energy phonon. Other third-order interaction processes involving zone center final states (i.e., polariton or photons) are allowed but are very unlikely because of the low density of final states compared to zone edge mechanisms and will not be considered here.[2]

In the most general approach one must also include the renormalization of the final phonon states due to their eventual interaction with photons. However, this only influences a very small part of the phonon dispersion curve in the center of the Brillouin zone and can thus be neglected.[23] The harmonic phonon Hamiltonian can thus be written

$$H_{\rm ph}=\sum_{i,k}\hbar\omega_{ik}b_{ik}^{\dagger}b_{ik}\ , \tag{4.3}$$

where the summation extends over all the i phonon branches except the i_0 one. $\hbar\omega_{ik}$ denotes the energy of the i phonon with wave vector k. Interaction of the polariton with a two-phonon band can occur through both the third-order mechanical anharmonicity (for its mechanical part) and through the second-order dipole moment (for its electrical part). For the former process the interaction Hamiltonian can be written[21]

$$H_{\rm int}^{M}=\sum_{\substack{i,j\\k,q}}3V_{ij}^{(3)}(k,q,-k-q)A_{i_0k}A_{iq}A_{j-k-q}\ . \tag{4.4}$$

$A_{iq}=(b_{iq}+b_{i-q}^{\dagger})$ is the vibration amplitude of the i phonon. The summation here extends over all the phonon modes and we have explicitly taken into account wave-vector conservation. Using the second-order dipole moment

$$P_2(k)=\sum_{i,j,q}M_{i,j}(k,q,-k-q)\frac{h}{2(\omega_{iq}\omega_{jk+q})^{1/2}}A_{iq}A_{j-k-q}, \tag{4.5}$$

the Hamiltonian of interaction of the photon part of the polarization takes a similar form:[23]

$$H_{\rm int}^{E}=\sum_{\substack{i,j\\k,q}}iD_{ij}^{(2)}(k,q,-k-q)\frac{\omega_{iq}}{(\omega_{i_0k}\omega_k)^{1/2}}A_kB_{iq}A_{j-k-q} \tag{4.6}$$

with $B_k=(a_k-a_{-k}^{\dagger})$ and a similar definition for the phonon operator B_{iq}. ω_k is the photon frequency $\omega_k=ck/(\epsilon_b)^{1/2}$ and the coupling constant $D^{(2)}$ is defined as

$$D_{ij}^{(2)}(k,q,-k-q)=2\left[\frac{2\pi h\omega_{i_0k}}{\epsilon_bV}\right]^{1/2}M_{ij}(k,q,-k-q)\ . \tag{4.7}$$

The interaction Hamiltonian can be rewritten in terms of polariton operators using the canonical transformations (4.2):

$$\begin{aligned}H_{\rm int}=&\sum_{i,j,k,\rho,q}3(-1)^{\rho+1}V_{ij}^{(3)}(k,q,-k-q)\\&\times[S_{\rho}^{M}(k)]^{1/2}A_{\rho k}A_{iq}A_{j-k-q}\\&+D_{ij}^{(2)}(k,q,-k-q)\omega_{iq}\frac{[S_{\rho}^{E}(k)]^{1/2}}{(\omega_{i_0k}\omega_{\rho k})^{1/2}}\\&\times B_{\rho k}B_{iq}A_{j-k-q}\ ,\end{aligned} \tag{4.8}$$

where $S_{\rho}^{M}(k)$ and $S_{\rho}^{E}(k)$ are, respectively, the phonon and photon strength factor of the ρ polariton with wave vector k.[1] They measure, respectively, the mechanical and electromagnetic energy content of the polariton and thus characterize its nature. The total Hamiltonian of the interacting system is given by

$$H=H_0+H_{\rm ph}+H_{\rm int} \tag{4.9}$$

from which the renormalized properties of the polariton can be calculated. The interacting polariton is described by the polariton propagator:[13]

$$G_{\rho k}=-i\Theta(t)\langle\langle[\alpha_{\rho k}(t),\alpha_{\rho k}^{\dagger}(0)]\rangle\rangle\ , \tag{4.10}$$

where $\Theta(t)$ is the step function and $\langle\langle\ \rangle\rangle$ means statistical average. Using the standard procedure[24] with the Hamiltonian (4.9) one obtains a Dyson equation for the Fourier component of the polariton propagator:

$$G_{\rho k}(\omega)=[(G_{\rho k}^{0})^{-1}-\Pi_{\rho k}]^{-1}\ , \tag{4.11}$$

where $G_{\rho k}^{0}$ is the bare polariton propagator,

$$G_{\rho k}^{0}=\frac{1}{2\pi}(\omega-\omega_{\rho k})^{-1}\ , \tag{4.12}$$

and $\Pi_{\rho k}$ is the polariton self-energy:

$$\begin{aligned}\Pi_{\rho k}=\frac{2\pi}{\hbar^2}\sum_{i,j,q}&\left[\frac{|6(-1)^{\rho+1}V_{ij}^{(3)}(k,q,-k-q)[S_{\rho}^{M}(k)]^{1/2}-(\omega_{iq}+\omega_{jk+q})D_{ij}^{(2)}(k,q,-k-q)[S_{\rho}^{E}(k)/\omega_{i_0k}\omega_{\rho k}]^{1/2}|^2}{2(\omega-\omega_{iq}-\omega_{jk+q})}\right.\\&\left.+\frac{|6(-1)^{\rho+1}V_{ij}^{(3)}(k,q,-k-q)[S_{\rho}^{M}(k)]^{1/2}+(\omega_{iq}+\omega_{jk+q})D_{ij}^{(2)}(k,q,-k-q)[S_{\rho}^{E}(k)/\omega_{i_0k}\omega_{\rho k}]^{1/2}|^2}{2(\omega+\omega_{iq}+\omega_{jk+q})}\right]\\&\times[1+n(\omega_{iq})+n(\omega_{jk+q})]\\&+\frac{|6(-1)^{\rho+1}V_{ij}^{(3)}(k,q,-k-q)[S_{\rho}^{M}(k)]^{1/2}+(\omega_{iq}-\omega_{jk+q})D_{ij}^{(2)}(k,q,-k-q)[S_{\rho}^{E}(k)/\omega_{i_0k}\omega_{\rho k}]^{1/2}|^2}{(\omega+\omega_{iq}-\omega_{jk+q})}\\&\times[n(\omega_{iq})-n(\omega_{jk+q})]\ .\end{aligned} \tag{4.13}$$

In optical experiments one accesses the polariton density of states $d_{\rho\kappa}(\omega)$ which is proportional to the imaginary part of the polariton propagator:

$$d_{\rho k}(\omega)=-\frac{1}{\pi}\mathrm{Im}G_{\rho k}(\omega)=\frac{-1}{2\pi^2}\frac{(2\pi)^{-1}\mathrm{Im}\Pi_{\rho k}(\omega)}{[\omega-\omega_{\rho k}-(2\pi)^{-1}\mathrm{Re}\Pi_{\rho k}(\omega)]^2+[(2\pi)^{-1}\mathrm{Im}\Pi_{\rho k}(\omega)]^2} . \tag{4.14}$$

The anharmonic interactions renormalize the polariton dispersion which is given by the maximum of the density of states[25] and introduce a polariton lifetime through the imaginary part of the self-energy. Assuming a weak perturbation the dispersion curve renormalization can be neglected and a Lorentzian broadening of the polariton is predicted with a linewidth directly proportional to the imaginary part of the self-energy:

$$\begin{aligned}\Gamma_\pi(\omega_{\rho k})=&\sum_{i,j,q}\Gamma^{-}_{ijqk}[1+n(\omega_{iq})+n(\omega_{jk+q})]\\&\times\delta(\omega_{\rho k}-\omega_{iq}-\omega_{jk+q})\\&+\Gamma^{+}_{ijqk}[n(\omega_{iq})-n(\omega_{jk+q})]\\&\times\delta(\omega_{\rho k}+\omega_{iq}-\omega_{jk+q}) ,\end{aligned} \tag{4.15}$$

where $n(\omega)$ is the Bose factor for the phonon of frequency ω. Taking into account the expression for the photon and phonon strength factor[1] the coupling coefficients are given by

$$\Gamma^{\pm}_{ijqk}=\frac{\pi}{\hbar^2}S^M_\rho(k)\left|6V^{(3)}_{ij}(k,q,-k-q)-D^{(2)}_{ij}(k,q,-k-q)\frac{\omega_0^2-\omega_{\rho k}^2}{\Omega_p\omega_0}\right|^2 . \tag{4.16}$$

The first term in (4.15) describes a down-conversion process where the initial polariton with wave vector k decays into two lower-energy phonons with wave vector q and $k-q$, respectively. The second term describes polariton down conversion where the initial excitation is scattered by a thermal phonon (i,q) into a phonon of higher energy $(j,k+q)$. The preceeding expression ensures wave-vector and energy conservation while symmetry conservation is included in the coupling factors. In their general form the coupling terms depend on two independent parameters describing, respectively, mechanical and electrical anharmonicity. If a dominant mechanical anharmonicity is assumed one obtains a polariton damping proportional to the parent phonon damping:

$$\Gamma_\pi=S^M_{\rho k}\Gamma_{\mathrm{ph}}(\omega_{\rho k}) , \tag{4.17}$$

where, noting that $k\sim 0$, the phonon damping takes its usual form but is calculated at the polariton energy:[21]

$$\Gamma_{\mathrm{ph}}=\frac{36\pi}{\hbar^2}\sum_{i,j,q}|V^{(3)}_{ij}(0,q,-q)|^2\{[1+n(\omega_{iq})+n(\omega_{jq})]\delta(\omega_{\rho k}-\omega_{iq}-\omega_{jq})+2[n(\omega_{iq})-n(\omega_{jq})]\delta(\omega_{\rho k}+\omega_{iq}-\omega_{jq})\} . \tag{4.18}$$

This approximation has been frequently used in previous experiments but, except close to the transverse mode, there is no clear reason to *a priori* neglect electrical anharmonicity. The relative contribution of these two terms depends on the investigated crystal and can lead to important modifications of the damping in the vicinity of a two-phonon band. In particular, for comparable mechanical and electrical anharmonicity destructive interferences can occur, strongly reducing the polariton damping rate. Cancellation of the coupling can be observed on either side of the forbidden band depending on the relative sign of $V^{(3)}$ and $D^{(2)}$. This interference effect is comparable to the one observed in the Raman intensity of the polariton (Sec. II). The Raman excitation of a polariton can be formally described as a particular three-particle interaction where two photons (or more exactly two polaritons in the medium) of high-energy interact to create a low-energy polariton. Although highly improbable the reverse process is a relaxation channel for a nonequilibrium polariton realizing energy, wave vector and symmetry conservation. Such an up conversion is formally equivalent to the three-particle interaction described above.

The frequency dependence of the polariton damping due to its change in nature is, however, not easy to identify because of the simultaneous variation of the density of accessible final states. If we assume wave-vector-independent anharmonic coefficients and a small dispersion of the final phonons, so that average phonon frequencies can be used, the polariton damping rate can be written

$$\begin{aligned}\Gamma_\pi=&\sum_{i,j}\Gamma^d_{ij}(\omega_{\rho k})[1+n(\omega_i)+n(\omega_j)]d_{\omega_i+\omega_j}(\omega_{\rho k})\\&+\Gamma^u_{ij}(\omega_{\rho k})[n(\omega_i)-n(\omega_j)]d_{\omega_j-\omega_i}(\omega_{\rho k}) ,\end{aligned} \tag{4.19}$$

where $d_{\omega_j\pm\omega_i}(\omega)$ is the density of states of the $\omega_i\pm\omega_j$ two-phonon band at the frequency ω and at $k=0$. $\Gamma^{d,u}_{ij}$ are average coupling coefficients. Discrimination between the frequency variation of the anharmonic coefficients and the frequency variation of the density of states is not straightforward and can be realized only if the two-phonon density of states is known from independent experiments.[26]

In infrared experiment this interference effect has already been pointed out in the frequency dependence of the absorption coefficient in the vicinity of a two-phonon band.[27] The results are best described in terms of the

imaginary part of the dielectric function which can be directly calculated from the photon Green's function. However, the correspondence between the temporal and spatial evolution of the polariton wave packet allows $\epsilon''(\omega)$ to be readily obtained from the polariton lifetime $T_1 = T_2/2$, using (2.5) and (2.6).[28] The result is formally identical to the expression deduced by Szigeti using a different approach.[27]

Because of the lack of theoretical and experimental information on phonon dispersion in $LiIO_3$ a quantitative interpretation of the frequency-dependent measurement of Sec. III including the variation of the coupling coefficient is not possible. We have thus interpreted our data in terms of global polariton relaxation as defined by (4.19). The shape of the frequency dependence of the dephasing rate can be approximated by estimating the number of accessible channels for the two third-order mechanisms using the known frequencies of the phonon at $k=0$. The results are plotted at the bottom and at the top of Fig. 8 for, respectively, the down- and up-conversion processes. Below the reststrahlen band both of the mechanisms are possible. The former corresponds mainly to polariton splitting into two phonons of comparable energy and the latter to scattering into one of the A, B, E_1, or E_2 symmetry stretching modes of the IO_3^- ion in the $\omega_{TO}-\omega_{LO}$ frequency region with simultaneous absorption of a thermal lattice phonon ($\sim 100\ cm^{-1}$). As the reststrahlen band under investigation is the highest one-phonon frequency region in $LiIO_3$ up conversion is not possible for polaritons above the longitudinal mode so that their dominant relaxation channel is down conversion into the $\omega_{TO}-\omega_{LO}$ region with emission of a lattice phonon ($\sim 100\ cm^{-1}$). Although the physical processes are different it is interesting to note that the $\omega_{TO}-\omega_{LO}$ region plays a role similar to the two-photon band in the case of polariton Fermi resonance, acting as a reservoir of accessible states for phonon-assisted up or down conversion of the polariton.[26] A good correlation between the number of relaxation channels and the measured dephasing rate is observed particularly if one considered that the main contributions come from the down-conversion processes at low temperatures. Although we have used a rough estimation of the density of accessible states this indicates that, as expected, third-order mechanisms dominate the relaxation.

The temperature dependence of the polariton decay rate is imposed by this interpretation which can thus be tested by performing temperature-dependent measurements. The temperature dependence of the polariton dephasing rate is included in the occupation numbers of the phonons involved in the processes. As the Bose factors are slowly varying functions of the phonon frequency and as the energies of the involved phonons are relatively close for the investigated polaritons a mean value $\bar{\omega}_i$ of the phonon frequencies can be used in (4.9). Below ω_{TO} the damping rate takes the form

$$\Gamma_\pi(\omega_\pi,T)=\gamma^d(\omega_\pi)[1+n(\bar{\omega}_1,T)+n(\bar{\omega}_2,T)] + \gamma^u(\omega_\pi)[n(\bar{\omega}_E,T)-n(\bar{\omega}_B,T)] \quad (4.20)$$

for the down conversion $\omega_\pi(k_\pi\sim 0)\rightarrow\omega_1(\mathbf{q})+\omega_2(-\mathbf{q})$ and for the up conversion $\omega_\pi(k_\pi\sim 0)+\omega_E(\mathbf{q})\rightarrow\omega_B(\mathbf{q})$. Above ω_{LO} we obtain

$$\Gamma_\pi(\omega_\pi,T)=\gamma^d(\omega_\pi)[1+n(\bar{\omega}_E,T)+n(\bar{\omega}_B,T)] \quad (4.21)$$

for the down-conversion mechanism $\omega_\pi(k_\pi\sim 0)\rightarrow\omega_E(\mathbf{q})+\omega_B(-\mathbf{q})$. γ^d and γ^u are frequency-dependent effective coupling parameters summing up all the contributions from, respectively, the down- and up-conversion processes.

Using these expressions we have fitted the measured temperature dependence of the polariton damping rate. This is exemplified in Figs. 9 and 10 for the 680- and 880-cm^{-1} polariton, respectively, below and above the forbidden band. For these particular frequencies the damping rate can be explicitly written

$$\Gamma_\pi(680)=\gamma^d(680)[1+2n(340)] + \gamma^u(680)[n(100)-n(780)]\ , \quad (4.22a)$$

$$\Gamma_\pi(880)=\gamma^d(880)[1+n(100)+n(780)]\ , \quad (4.22b)$$

where the polariton frequency and the average phonon frequencies are given in wave numbers. The phonon occupation numbers are negligible at low temperature ($T<10$ K) so that the γ^d factors are fixed by the low-temperature data. For the 880-cm^{-1} polariton there is thus no real fitting parameter. Nevertheless a very good agreement is obtained between the measured and theoretical temperature variation (full line in Fig. 10). A similar agreement is obtained for the 680-cm^{-1} polariton using γ^u as a fitting parameter.

With the same procedure we have fitted the temperature dependence of the dephasing rates over the whole frequency and temperature range investigated (from 10 K to room temperature). A similar agreement is obtained and the frequency variations of the up- and down-conversion coupling parameters are shown in Fig. 11. A good correlation with the number of allowed relaxation channels is observed with a smaller variation for γ^u than

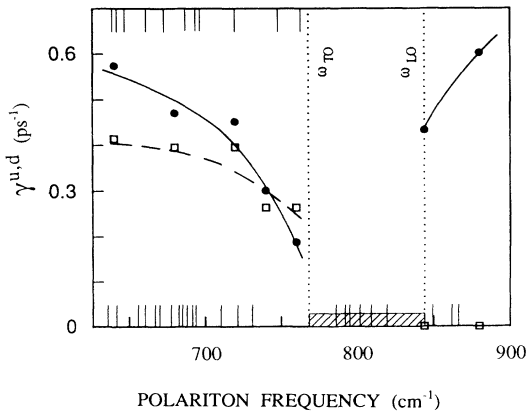

FIG. 11. Measured dispersion of the anharmonic coefficients, γ^u and γ^d [(4.20) and (4.21)], describing polariton up and down conversion (squares and points respectively) in $LiIO_3$. The full and dashed lines are guides to the eye. The small lines at the bottom (top) of the figure indicate the allowed down- (up-) conversion processes.

for γ^d in the vicinity of ω_{TO} and no contribution of γ^u above ω_{LO}. This agreement and the close description of the temperature-dependent measurements provide an obvious confirmation of the interpretation of polariton relaxation given above.

V. CONCLUSION

The application of the nonlocal time-resolved CARS technique to the investigation of a phonon polariton has been described using a classical model. The results show that for a sufficient frequency selectivity the group velocity concept can be applied. For wave-packet propagation over short distances extrinsic decay processes can be neglected and the temporal and spatial evolution of the polariton is dominated by its intrinsic dephasing. Both of these parameters governing the excitation dynamics are independently accessed in the time domain allowing in particular a direct measurement of the dispersion of the polariton dephasing time.

The possibility of measuring both the temperature and frequency signatures of the polariton dephasing rate allows a precise analysis of the anharmonic interactions in the crystal.[26] This point is of particular interest since in usual experiments on phonons one only accesses the temperature signature of the relaxation channel. This information is frequently insufficient for a precise determination of the actual decay channel leading sometimes to ambiguous interpretation of the data.[29] The ability of discriminating the contribution of the different interaction processes between quasiparticles using the polariton concept has also been illustrated in recent time-resolved experiments on the exciton polariton.[30]

The model has been used to analyze the measurements performed on the ordinary polarization in lithium iodate. The results of the direct measurements of the polariton group velocity are in very good agreement with the estimations from the static investigations. The polariton relaxation has been described using a theoretical analysis including both the mechanical and electrical anharmonicity. The model predicts a Lorentzian broadening of the excitation, in agreement with the experimental results, and that destructive interferences between these two interaction processes can be observed. Provided that the phonon dispersion curves are known, the mechanical and electrical anharmonic contributions can be separated using polariton relaxation. The lack of such information in lithium iodate has prevented a quantitative interpretation of the measurements, and only a qualitative interpretation of the frequency dependence of the dephasing rate has been given. The relaxation is here dominated by population relaxation processes induced by three-particle interactions. As expected in good-quality crystals pure dephasing which involves higher-order anharmonic processes can be neglected. Interpretation of the data is confirmed by the temperature-dependent measurements.

The nonlocal time-resolved CARS allows the tracking of the excited polariton wave packet at any point inside the crystal and in that sense constitutes a powerful tool for the investigation of polariton evolution in the real time and space under various conditions, including scattering by impurities or interactions with boundaries. In particular, one can locally probe polariton reflection and transmission at an interface.[31] Similar methods could be applied to the investigation of other propagating modes of solids and in particular to surface excitations.

[1] D. L. Mills and E. Burstein, Rep. Prog. Phys. **37**, 817 (1974).
[2] C. Mavroyannis and K. N. Pathak, Phys. Rev. **182**, 872 (1969); C. Mavroyannis, Phys. Rev. B **3**, 2750 (1971).
[3] Y. N. Polivanov, Usp. Fiz. Nauk **126**(10), 185 (1978) [Sov. Phys. Usp. **21**, 805 (1978)].
[4] S. Ushioda, J. D. McMullen, and M. J. Delaney, Phys. Rev. B **8**, 4634 (1973).
[5] D. M. Auston and M. C. Nuss, IEEE J. Quantum Electron. **24**, 184 (1988).
[6] G. M. Gale, F. Vallée, and C. Flytzanis, Phys. Rev. Lett. **57**, 1867 (1986).
[7] Y. Masumoto, S. Shionoya, and T. Takagahara, Phys. Rev. Lett. **51**, 923 (1983).
[8] M. van Exter and A. Lagendijk, Phys. Rev. Lett. **60**, 49 (1988).
[9] P. C. M. Planken, L. D. Noordam, J. T. M. Kennis, and A. Lagendijk, Phys. Rev. B **45**, 7106 (1992).
[10] L. A. Kulevsky, Y. N. Polivanov, and S. N. Poluektov, J. Raman Spectrosc. **3**, 239 (1975).
[11] C. H. Henry and C. G. B. Garrett, Phys. Rev. **171**, 1058 (1968).
[12] A. S. Barker and R. Loudon, Rev. Mod. Phys. **44**, 18 (1972).
[13] J. H. J. Benson and D. L. Mills, Phys. Rev. B **1**, 4835 (1970).
[14] A. Laubereau and W. Kaiser, Rev. Mod. Phys. **50**, 607 (1978).
[15] J. M. Crettez, J. P. Misset, and E. Coquet, J. Chem. Phys. **70**, 4194 (1979).
[16] F. Cerdeira, F. E. A. Melo, and V. Lemos, Phys. Rev. B **27**, 7716 (1983).
[17] F. E. A. Melo, F. Cerdeira, and V. Lemos, Solid State Commun. **41**, 281 (1982).
[18] V. N. Denisov, B. N. Mavrin, and V. B. Podobedov, Phys. Rep. **151**, 1 (1987).
[19] O. A. Doil'nitsyna and Y. N. Polivanov, Kvant. Elektron. (Moscow) **11**, 2177 (1984) [Sov. J. Quantum Electron. **14**, 1452 (1984)].
[20] G. M. Gale, F. Vallée, and C. Flytzanis, in *Dynamics of Molecular Crystals,* edited by J. Lascombe (Elsevier, Amsterdam, 1987), p. 81.
[21] S. Califano, V. Schettino, and N. Neto, in *Lattice Dynamics of Molecular Crystal,* edited by S. Califano, V. Schetlino, and N. Neto, Lecture Notes in Chemistry Vol. 21 (Springer-Verlag, Berlin, 1981).
[22] J. J. Hopfield, Phys. Rev. **112**, 1555 (1958).
[23] I. J. Lalov and K. T. Stoychev, Bulg. J. Phys. **6**, 305 (1979).
[24] P. C. K. Kwok, in *Solid State Physics: Advances in Research and Applications,* edited by F. Seitz, D. Turnbull, and H. Ehrenreich (Academic, New York, 1967), Vol. 20, p. 297.
[25] V. N. Agranovitch and I. J. Lalov, Usp. Fiz. Nauk **146**, 267 (1985) [Sov. Phys. Usp. **28**, 484 (1985)].
[26] F. Vallée, G. M. Gale, and C. Flytzanis, Phys. Rev. Lett. **61**, 2102 (1988).

[27]B. Szigeti, in *Lattice Dynamics,* edited by R. F. Wallis (Pergamon, New York, 1965), p. 337.
[28]R. Loudon, J. Phys. A **3**, 233 (1970).
[29]G. M. Gale, P. Schanne, and P. Ranson, Chem. Phys. **131**, 455 (1989).
[30]F. Vallée, F. Bogani, and C. Flytzanis, Phys. Rev. Lett. **66**, 1509 (1991).
[31]F. Vallée and C. Flytzanis (unpublished).